

# The Geothermal Artificial Intelligence for geothermal exploration

Moraga, J.<sup>1,\*</sup>, Duzgun, H.S. <sup>2</sup>, Cavur, M. <sup>3</sup>, Soydan, H. <sup>4</sup>

## Abstract

Exploration of geothermal resources involves analysis and management of a large number of uncertainties, which makes investment and operations decisions challenging. Remote Sensing (RS), Machine Learning (ML) and Artificial Intelligence (AI) have potential in managing the challenges of geothermal exploration. In this paper, we present a methodology that integrates RS, ML and AI to create an initial assessment of geothermal potential, by resorting to known indicators of geothermal areas namely mineral markers, surface temperature, faults and deformation. We demonstrated the implementation of the method in two sites (Brady and Desert Peak geothermal sites) that are close to each other but have different characteristics (Brady having clear surface manifestations and Desert Peak being a blind site). We processed various satellite images and geospatial data for mineral markers, temperature, faults and deformation and then implemented ML methods to obtain pattern of surface manifestation of geothermal sites. We developed an AI that uses patterns from surface manifestations to predict geothermal potential of each pixel. We tested the Geothermal AI using independent data sets obtaining accuracy of 92-95%; also tested the Geothermal AI trained on one site by executing it for the other site to predict the geothermal / non-geothermal delineation, the Geothermal AI performed quite well in prediction with 72-76% accuracy.

## Keywords

- Geothermal Exploration; Machine Learning; Artificial Intelligence; Automated Labeling; Geophysics for Exploration; Geothermal Energy

## Highlights

- Novel deep learning model uses geological and geophysical information as data source
- Automated labeling process using unsupervised learning for training, and testing
- Preprocessing to create input and label layers for the deep learning model
- Artificial intelligence using independent data sets obtained accuracy of 92-95%

## DOI

[10.1016/j.renene.2022.04.113](https://doi.org/10.1016/j.renene.2022.04.113)

---

<sup>1</sup> Department of Mining Engineering, Colorado School of Mines, 1610 Illinois St., Golden, CO 80401, USA

\* [jmoraga@mines.edu](mailto:jmoraga@mines.edu)

<sup>2</sup> Fred Banfield Distinguished Endowed Chair and Professor, Mining Engineering, Colorado School of Mines, Golden, CO 80401, USA

<sup>3</sup> Management Information Systems Department, Kadir Has University, İstanbul 34083, Turkey

<sup>4</sup> Department of Mining Engineering, Colorado School of Mines, 1610 Illinois St., Golden, CO 80401, USA

## List of Abbreviations

Abbreviation	Meaning
<b>AI</b>	Artificial Intelligence
<b>AOI</b>	Area of Interest
<b>CNN</b>	Convolutional Neural Network
<b>DLM</b>	Deep Learning Model
<b>LCOE</b>	Levelized cost of Energy
<b>MADS</b>	Model Analysis and Decision Support
<b>ML</b>	Machine Learning
<b>NMF</b>	Non-negative matrix factorization
<b>PSInSAR</b>	Persistent Scatterer Interferometric Synthetic Aperture Radar
<b>RS</b>	Remote Sensing
<b>SAR</b>	Synthetic Aperture Radar
<b>SOM</b>	Kohonen's Self Organizing Map
<b>WACC</b>	Weighted Average Cost of Capital
<b>WoE</b>	Weight of Evidence

## 1. Introduction

Motivated by climate change, and international agreements like the Paris Agreement (1) and the United Nations Sustainable Development Goal 7 (SDG7) (2), nations are moving towards renewable energy. Despite the low environmental impact, reduced carbon footprint, and the economic competitiveness of geothermal energy, it has had limited investment. Geothermal energy constitutes only 0.19% of electricity capacity installed in 2019, and 0.33% of electricity generation in 2018 (1). There are various critical strategic factors limiting the adoption of geothermal energy. The resource availability (for example, zone belonging to the ring of fire (3)), political, legal and consumer understanding of technology (4), investment risk, and the levelized cost of energy (LCOE) as compared to local alternatives (5) are among the major factors. LCOE methodology provides disaggregation of costs and assessment of risks by weighting total costs over the life of the asset (6) and shows the competitiveness of the geothermal energy with other alternatives. However, as it is indicated by IRENA's Power Generation Costs 2019 report (7), LCOE does not properly capture the effects of risks in the economic analysis because of selection bias, which emerges from consideration of costs of only completed projects.

Most of the costs and associated risks in a geothermal project come out during the initial stages of the projects. Over 80% of LCOE is driven by capital costs (6), and exploration accounts for around 5% of the costs. However, these costs drive up to 54% of the total cost of preparation and drilling. Managing those costs and risks requires careful use of a phased exploration program (8) to maximize return on investment potential, especially at the earlier stages of the project (9). There are different approaches proposed for managing the associated risks. Sanchez-Alfaro et al. uses a variable Weighted Average Cost of Capital (WACC) that ranges between 9 and 15% to address the economic impact of this risk and mitigation strategies by country (for example, subsidies and risk capital in New Zealand) (4). Van der Zwaan penalizes geothermal WACC by 2% over other renewables, indicating that this is an assumption and an open area of research (10). The risk is especially severe in greenfield areas, where there is no basis for evaluation, and this has been mitigated by the efforts of governmental organizations (e.g., Iceland, New Zealand, USA, and Chile). Nevertheless, to expand the adoption of geothermal energy requires effort to mitigate the uncertainties associated with resource evaluation and exploration (including options like government-backed risk insurance) (11).

Exploration of geothermal resources involves analysis and management of a large number of uncertainties, which makes investment and operations decisions challenging. These uncertainties can be grouped as geological, technological and economic uncertainties. The geological uncertainty is inherent to the nature of the problem. The geological model of the geothermal site, which directly impacts the production strategy is highly dependent on the management of these uncertainties (Figure 1). The geological uncertainty stems from incomplete knowledge of subsurface characteristics of geothermal systems, namely geological setting, geomechanical properties, fracture distribution and permeability and spatiotemporal distribution of temperature. Additionally, a considerable amount of uncertainty is introduced through data acquisition and processing (objective uncertainty), the interpretation (subjective uncertainty), via the data analysis, modeling and interpretation (12). Technological uncertainties relate to the reservoir model, which is interlinked with geological model and the production strategy (Figure 1). The limitations in type of data available (most of the data comes from surface, and subsurface data is limited), the inherent statistical nature of the analysis, data resolution and error introduced by measurements and sensors and their interaction with the environment (e.g., clouds, noise, unavailability of day or night data, signal mixing, and data correction) constitute the sources of technological uncertainties. Economic uncertainties are interrelated with geological and technological uncertainties and impact the risk analyses, decision process, field development and production strategy (Figure 1). The main sources

of economic uncertainties are the inability to properly forecast the economic risk, value and costs, due to technical and geologic uncertainties, changes in energy technology, supply and demand of energy in time, competition, cost of capital (e.g., what is the associated technology or geological risk, as a percentage of weighted average cost of capital).

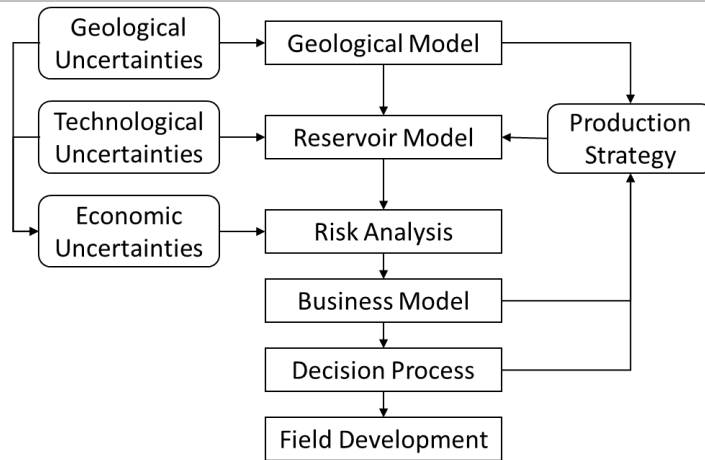


Figure 1 — Relationships between uncertainty and risk in resource evaluation and development (adapted from Witter et al. (12))

Therefore, several models and approaches (e.g., geological, geophysical, geochemistry and drilling technologies) are required to be integrated to manage the cost and uncertainty in geothermal projects. Remote sensing (RS) presents a unique opportunity to streamline and reduce the cost at each stage of the development of a geothermal project (preliminary survey and site selection, exploration, test drilling, geothermal field development, power plant design, commissioning and operation) (13). For example, the surface manifestations of geothermal sites can be analyzed through remote sensing data including surface deformation associated to geothermal activity using SAR interferometry, gaseous emissions, structural analysis, mineral mapping, temperature, heat flux measurement, and geobotany. These remote sensing techniques can play a role in exploration and reconnaissance, allowing for hydrogeological modeling, initial geochemical characterization (by mapping anomalous hydrothermal alterations), identification of fumaroles and hot springs through infrared analysis and surface topography, and others (12). However, compiling all the information obtained from surface manifestations to obtain thorough knowledge about the occurrence of geothermal sites requires large amount of expertise. Moreover, hidden relations in the data cannot be obtained by replicating the information to other sites.

Artificial Intelligence (AI) is a promising area for managing the challenges of geothermal exploration. Faulds et al. first introduced play fairway analysis (14) for the regional evaluation of geothermal potential, based on subsurface and surface data, and has incorporated machine learning (ML) to replicate the results of human evaluation of play fairway (15). There also exist a large amount of research in remote sensing applications in geothermal exploration. For example, Miyazaki used thermal infrared, airborne SAR, and satellite data to map potential geothermal resources (16), Littlefield and Calvin used a spectrometer to identify and to map geothermal indicator minerals (17), and Calvin and Pace used a portable spectrometer in drill cores for the same purpose (18). Fuzzy logic was used by Sadeghi and Khalajmasoumi for regional evaluation of geothermal potential (19). A comprehensive review of remote sensing applications for geothermal exploration is presented by Van der Meer et al. (13).

Machine learning has been used extensively in the late stages of geothermal exploration (20) (especially in geophysical (21) (22) and geochemical interpretation (23) (24)) and production (25) (26), but research on early stages of exploration is limited. A review of uses of ML in the geothermal production life cycle is given in (27) and (28).

For early exploration targeting, Vesselinov et al. applied Negative Matrix Factorization (NMF) and NMF coupled with a custom semi-supervised k-means algorithm (NMFk) in large-scale datasets (29) to identify the dominant features, optimize number of clusters and identify hidden signals in New Mexico (30), Great Basin (31), Hawaii (32), and Utah (33). This research points to the most relevant factors by area to consider in order to evaluate geothermal potential in a region, and the need to apply these factors for geothermal prospecting through machine learning approaches.

Faulds et al. (15), and Smith et al. (34), introduce machine learning and play fairway analysis from petroleum exploration to characterize geothermal signatures regionally, use a permutation supervised module to replicate previous work, and then incorporate Principal Component Analysis (PCA) and k-means (PCAk) to demonstrate a pipeline of unsupervised feature selection and semi-supervised clustering technique applied to the problem.

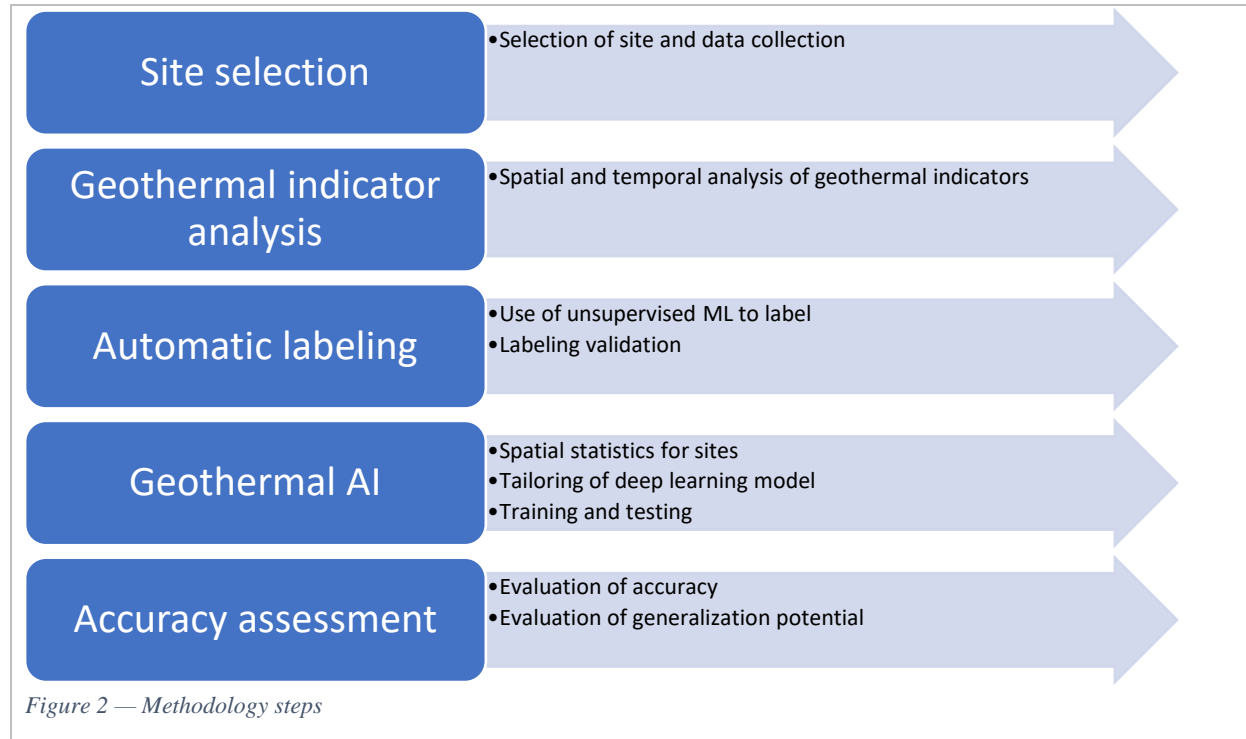
However, a comprehensive approach to the evaluation of geothermal potential at a local level using remote sensing, ML and AI is missing. Such an approach is extremely useful for reducing the cost and managing the risks related to the geothermal projects.

In this paper, we present a methodology that integrates RS, ML and AI to create an initial assessment of geothermal potential, by resorting to known indicators of geothermal areas namely mineral markers, surface temperature, faults and deformation. We demonstrated the implementation of the method in two sites (Brady and Desert Peak geothermal sites) that are close to each other but have different characteristics. We processed various satellite images and geospatial data for mineral markers, temperature gradient, faults and deformation and then implemented ML methods to obtain patterns of surface manifestations of geothermal sites. We developed an AI that uses these patterns of surface manifestations to predict the geothermal sites. Any AI system for geothermal exploration necessitates labeling of large number of data sets for the geothermal and non-geothermal areas to train and test the system. However, labeling geothermal sites by the use of expert knowledge is not practical as the process needs involvement of a large number of experts, who have in-depth knowledge on the sites. In order to tackle the problem of labeling we first developed an automatic labeling method using unsupervised ML before developing the AI system called Geothermal AI. Finally, we tested the Geothermal AI using independent data sets obtained from each site. Moreover, we tested the Geothermal AI trained on one site by executing it for the other site to predict the delineation of the surface footprints of the considered sites. Although both sites are different from each other in terms of resource characteristics (Brady having clear surface manifestations and Desert Peak being a blind site), the Geothermal AI performed quite well in prediction.

## 2. Methodology

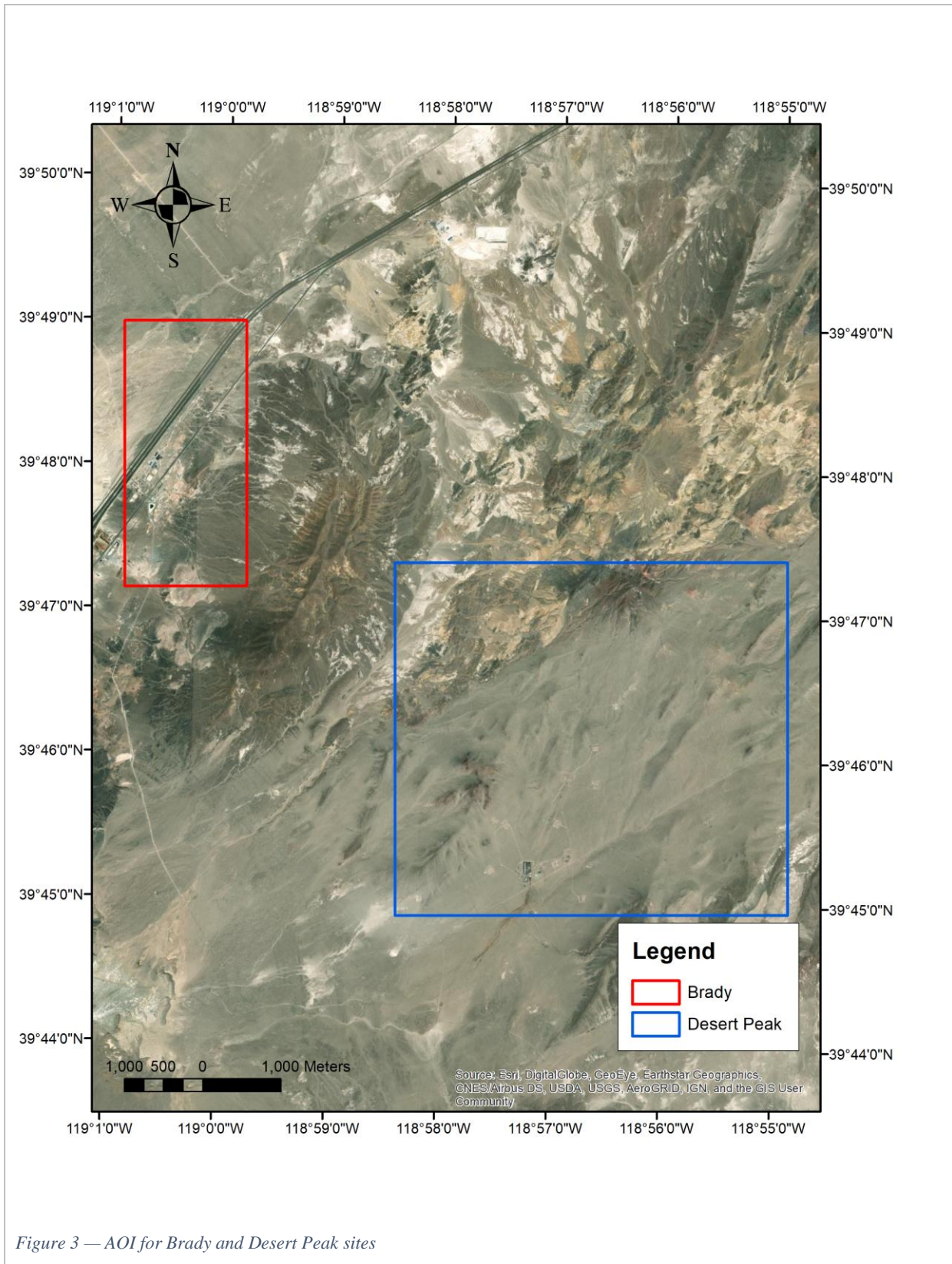
The proposed methodology consists of five stages (Figure 2). The first stage in the development of an AI system for geothermal exploration is the selection of inputs that help delineate the area with respect to geothermal potential (Figure 2). For this purpose, we selected two sites: the Brady and Desert Peak geothermal sites and collected data for geothermal indicators for these sites. The second stage of the methodology is the analysis of geothermal indicators, which includes spatial and temporal analysis of geothermal indicators using ML (Figure 2). The analysis of indicators using ML provides extraction of

patterns in each geothermal indicator data, which enhances learning process to be used in AI system. The third stage is the automatic labeling, which uses unsupervised ML algorithms to identify geothermal and non-geothermal sites to be used in training the AI system (Figure 2). The fourth stage is the development of the AI system, called Geothermal AI (Figure 2). The Geothermal AI relies on a deep learning algorithm which is tailored for the data characteristics of the geothermal sites using spatial statistics related to the considered sites. This stage also consists of training and testing the Geothermal AI using the Brady site. The final stage of the methodology is assessment of accuracy (Figure 2), In this stage we tested the Geothermal AI trained on one site by executing it for the other site to predict the delineation of the surface footprints of the considered sites.



### 2.1. Site selection

The Brady Hot Springs Geothermal area is located North East from Fernley, NV, and is part of Nevada's Northwest Basin and Range Geothermal Region. In this area, there are geothermal operations in two sites, Brady (39.79°N, 119.02°W) and Desert Peak (39.75°N, 118.95°W). This area has been extensively studied and explored, and there is a broad amount of data available through the Open Energy Information (OpenEI) and its Geothermal Data Repository (35) (36). The location of Brady and Desert Peak is illustrated in Figure 3 and we collected data associated to these areas of interest (AOI) from several sources (Table 1), which is explained in the next section.



The data is further analyzed to extract meaningful information that will constitute the basis for the input layers of the Geothermal AI which uses a deep learning model (DLM).

## 2.2. Geothermal indicators analysis

In order to identify geothermal indicators to be used in the Geothermal AI, we conducted an extensive literature survey. Geothermal exploration is a multi-step process which goes from regional to local analysis. The regional to local scale analyses are required to determine overall potential and to finalize a resource and reserve model for the geothermal system. The first step is a desktop analysis where bibliographic research is done in the area of interest, where maps and analyses from the region are acquired and include topographical, geological, geophysical, geochemical, thermal, hydrological, tectonic, seismic, gravitational, magnetic, land rights, supply/demand and other data. This quantitative, qualitative and interpreted data is used to assess the regional geothermal potential of an area, and its initial feasibility from an economic, logistical, regulatory, legal and technical standpoint (37) (13) (38) (39) (40). Several of these factors can also be analyzed using remote sensing and assessed statistically to identify potential (13) (41) (42), including geochemical (e.g., hydrothermal mineral alterations) (42) (43) (44) (45), geological characteristics (e.g., faults, lithology and stratigraphy, seismicity, volcanism) (13) (46) (47), geophysical manifestations and anomalies (e.g., Bouguer anomalies, magnetic, hydrology and aquifers, deformation) (48) (49) (50) (51), and geothermal anomalies (e.g., thermal flux, hot springs, and fumaroles) (52) (53). Of these indicators, we selected those that have satellite data openly available with sufficient resolution for developing a low-cost Geothermal AI. These include temperature (e.g., detection of fumaroles or thermal anomalies) (54) (14), mineral alterations (54) (55), faults (38) (56) (57), and deformation (58) (59). Table 1 lists the selected indicators and associated data sources and characteristics

Table 1 — Data sources for the considered geothermal indicators

Indicator	Data	Data source	Resolution	Number of Pixels	Time Span
Temperature	Land surface temperature	LANDSAT	30 m	2.5E+07	05/2018 – 10/2020
Fault density	Fault map	Nevada Geological Survey	n/a		
Mineral markers	Hyperspectral images	HyMap	3 m	2.1E+07	June 2003
Deformation	Synthetic Aperture Radar (SAR)	Sentinel-1	5 x 20 m	2.9E+08	12/2017 – 12/2019

The literature survey also shows successful use of RS, ML and AI in geological and geophysical analyses. An overview of AI in renewable energy to identify resources and improve technology, environmental awareness and improvement of distribution systems and management is given by (60) and (61). Clustering analysis of multispectral and hyperspectral data (62) (63), satellite image segmentation (64), and time-series analysis (65) (66) (67) are the examples of ML and RS analyses.

As a result of this extensive literature survey, we identified ML methods that reveal patterns for each geothermal indicator. A high-level description of the ML methods used for each indicator is given below:

**Temperature:** It is known from the literature survey that geothermal resources exhibit some characteristic surface temperature patterns. To extract these patterns, we analyzed 25 LANDSAT 8's

Level-2 Provisional Surface Temperature product images between 2018 and 2019 to determine persistently hot zones in the selected sites. Several ML methods have been used in the literature for time-series (68) and clustering analyses (e.g., self-organizing maps (SOM) and k-means clustering) showing their potential for spatial data. The k-means clustering algorithm is one of the most well-known unsupervised algorithms used for extracting spatial patterns. The first step in k-means is to calculate the  $k$  centroids. In the second step, the nearest centroid location for each data point is found by using the distance metrics. We obtained persistently hot zones for the selected sites using k-means clustering. After several trials of  $k$  values, we extracted the pattern of persistently hot zones in time with the  $k$  value of five. We used pixel voting to select the most anomalous pixels by assigning values that represent the number of instances a pixel was selected in the top two hottest classes. Our analysis is dynamic and searches for anomalies in time. The approach is to look at, at least, one full year of data and cluster with k-means, isolating as anomalies the high temperature areas (relative to each snapshot in time); because it looks at time-based anomalies and relative temperatures, the approach is valid regardless of climate, weather or seasonality, given that even though climate changes, there are persistent hot zones (69) unless there is permanent impact due to changes in vegetation, cold water accumulation, or the site is completely blind (for example, no hot zones because of subsurface cold water reservoir) (70).

**Faults:** The pattern and intensity of faults presents characteristic features for the geothermal resources. We obtained fault maps for Brady (57) and Desert Peak (56), in shapefiles, where the faults are indicated in terms of linear features. We converted fault lines into a density map so that we can incorporate the influence area of the faults in the Geothermal AI system.

**Mineral Markers:** Hydrothermally altered minerals are generated as a result of minerals exposure to water at high temperature. These minerals surface by means of faults, hot springs and fumaroles, and their chemical characteristics become then a signature of the probable underground system characteristics (43) (42). The discharge of geothermal fluids on the surface can form mineral deposits of siliceous sinters and travertine (71), borates (72), sulfates and chlorides (53), with calcite and quartz encompassing minerals formed at temperatures from 100 to more than 300 °C (40). For the area of interest Kratt (54) (55), and in the overall region Littlefield & Calvin (17), have described the occurrence of Kaolinite, Calcite (Tufa), Sinter deposits (Opal-A, Opal-CT, Chalcedony and Quartz), Hematite, Epsomite, Gypsum and other relevant hydrothermally altered minerals. From this list, we selected minerals from the region that indicate geothermal alteration, which are present in the selected sites, and their spectral signatures are available in the USGS Spectral Library (73). These include Chalcedony, Opal-A, Opal-C, Kaolinite, Gypsum, Hematite and Epsomite. Of those, Chalcedony, Opal, Kaolinite and Gypsum spectra were used to perform Spectral Analysis and obtain maps indicating presence of those minerals (Epsomite was not selected due to sparsity of its presence). We used the hyperspectral satellite images (Table 1) and adopted the target detector process in the ENVI software package (74). The eight algorithms available were used (75) by first creating a Minimum Noise Fraction (MNF) transform with co-variance, these are: **Adaptive Coherence Estimator (ACE)** (76), which is derived from the Generalized Likelihood Ratio (GLR) (77) approach, it does not require knowledge of all the endmembers within a scene; **Constrained Energy Minimization (CEM)** (78), CEM uses a finite impulse response (FIR) filter to pass through the desired target while minimizing its output energy resulting from backgrounds other than the desired targets; **Matched Filtering (MF)** (79), finds the abundance of targets using a partial unmixing algorithm, MF is a mean-centered version of CEM where the data mean is subtracted from all pixel vectors; **Orthogonal Subspace Projection (OSP)** (80), OSP first designs an orthogonal subspace projector to eliminate the response of non-targets, then applies MF to match the desired target from the data, it requires the

definition of more than one target spectra; **Spectral Angle Mapper (SAM)** (81) matches image spectra to reference target spectra in n dimensions. SAM compares the angle between the target spectrum and each pixel vector in n-dimensional space, where smaller angles represent closer matches to the reference spectrum; **Mixture Tuned Matched Filtering (MTMF)** (82), MTMF uses the MNF transform input file to perform MF, and it adds an infeasibility image to the results (Pixels with a high infeasibility are likely to be MF false positives); **Target-Constrained Interference-Minimized Filter (TCIMF)** (83), TCIMF detects the desired targets, eliminates non-targets, and minimizes interfering effects in one operation, TCIMF can potentially reduce the number of false positives over CEM results; **Mixture Tuned Target-Constrained Interference-Minimized Filter (MTTCIMF)** (84), this method combines the Mixture Tuned technique and TCIMF target detector, creates an infeasibility image and uses it to reduce the number of false positives that are sometimes found when using TCIMF alone, when non-target spectra are specified, MTTCIMF can potentially reduce the number of false positives over MTMF. We fused the resulting mineral maps from each of the eight methods by voting (85) to obtain a “Mineral Markers” map indicating the presence of one or more of the alteration minerals in the area.

**Deformation:** Occurrence of deformation in the form of subsidence and uplift for geothermal sites is highly investigated topic in the literature. Cavur et al (59) provide an overview of these studies for the considered sites. These deformations are mainly due to the pore pressure changes and thermal contraction. We used this indicator to establish ground truth with respect to the location and extent of the geothermal system being exploited both in Brady, and the blind geothermal system in Desert Peak. As given in Table 1, Sentinel-1 data was acquired for the period from December 2017 to December 2019, and 59 high quality images were used as input for Persistent Scatterer Interferometric Synthetic Aperture Radar (PSInSAR) analysis using the SARPROZ application (86). Using Self Organizing Maps, the time series results from PSInSAR were classified based on their behavior in time, to ensure that there was no bias introduced by the selection of the time period. The resulting clusters were reduced to three classes (Stable, Subsidence and Uplift). Details of deformation analyses can be found in (59). The Subsidence and Uplift layers were turned into two more inputs for our labeling algorithm.

The results of the ML methods for each indicator constitute the input data of the automatic labeling and the Geothermal AI system. Figure 4 (a) shows the resulting layers for Brady Hot Springs, while Figure 4 (b) shows the same layers for Desert Peak.

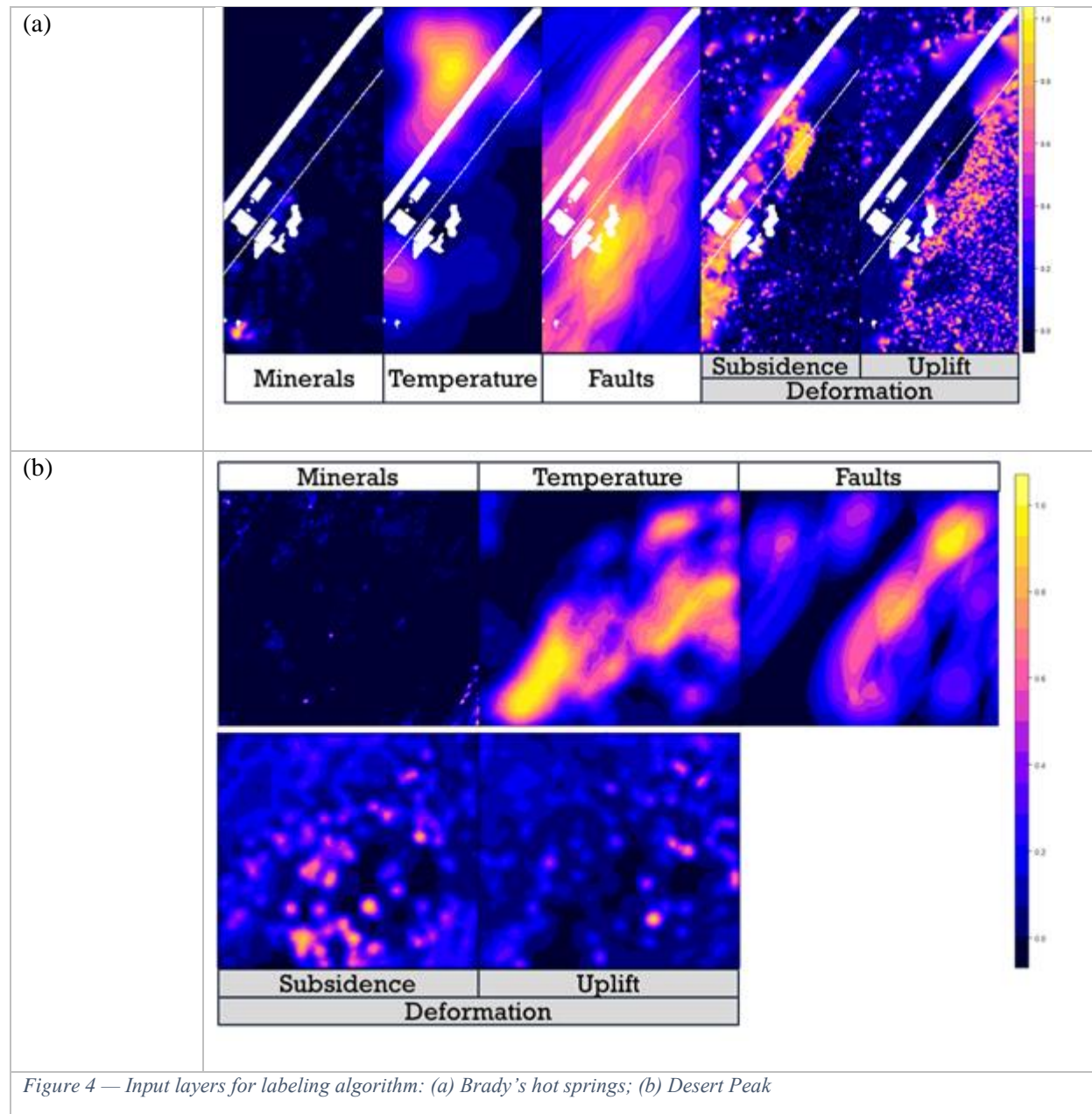
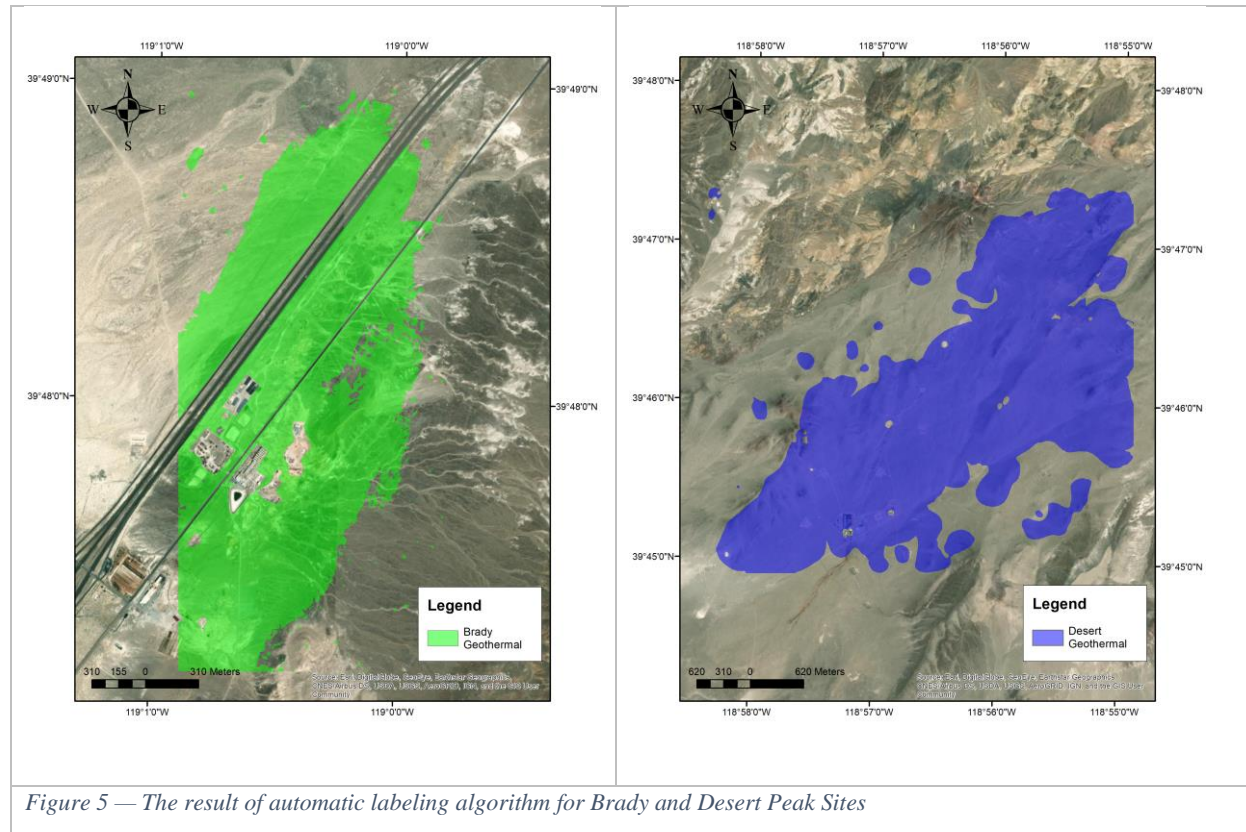


Figure 4 — Input layers for labeling algorithm: (a) Brady's hot springs; (b) Desert Peak

### 2.3. Automatic labeling

Labeling the geothermal system is a complex endeavor given the uncertainty and the need for expert interpretation. An automatic labeling with elimination of the expert input can be achieved by using unsupervised, self-supervised or weakly-supervised methods (87). It is known that operating geothermal sites are subject to deformation (59). Nevertheless, solely using deformation as the labeling system may create false negative labeling by omitting areas that may not show subsidence but actually belong in the actively exploited geothermal system. To eliminate this problem, we used five (temperature, faults, mineral markers, subsidence and uplift) of the geothermal indicators to delineate the surface footprint of the geothermal resource in the considered sites. For this purpose we applied an unsupervised clustering

algorithm, Kohonen's self-organizing maps (SOM) (88). In SOM we build 25 clusters based on the five multi-variate data layers (temperature, faults, mineral markers and deformation). We later grouped the resulting clusters into two classes that represent "Geothermal" (a value of 1) and "Non-geothermal" (a value of 0) as shown in Figure 5.

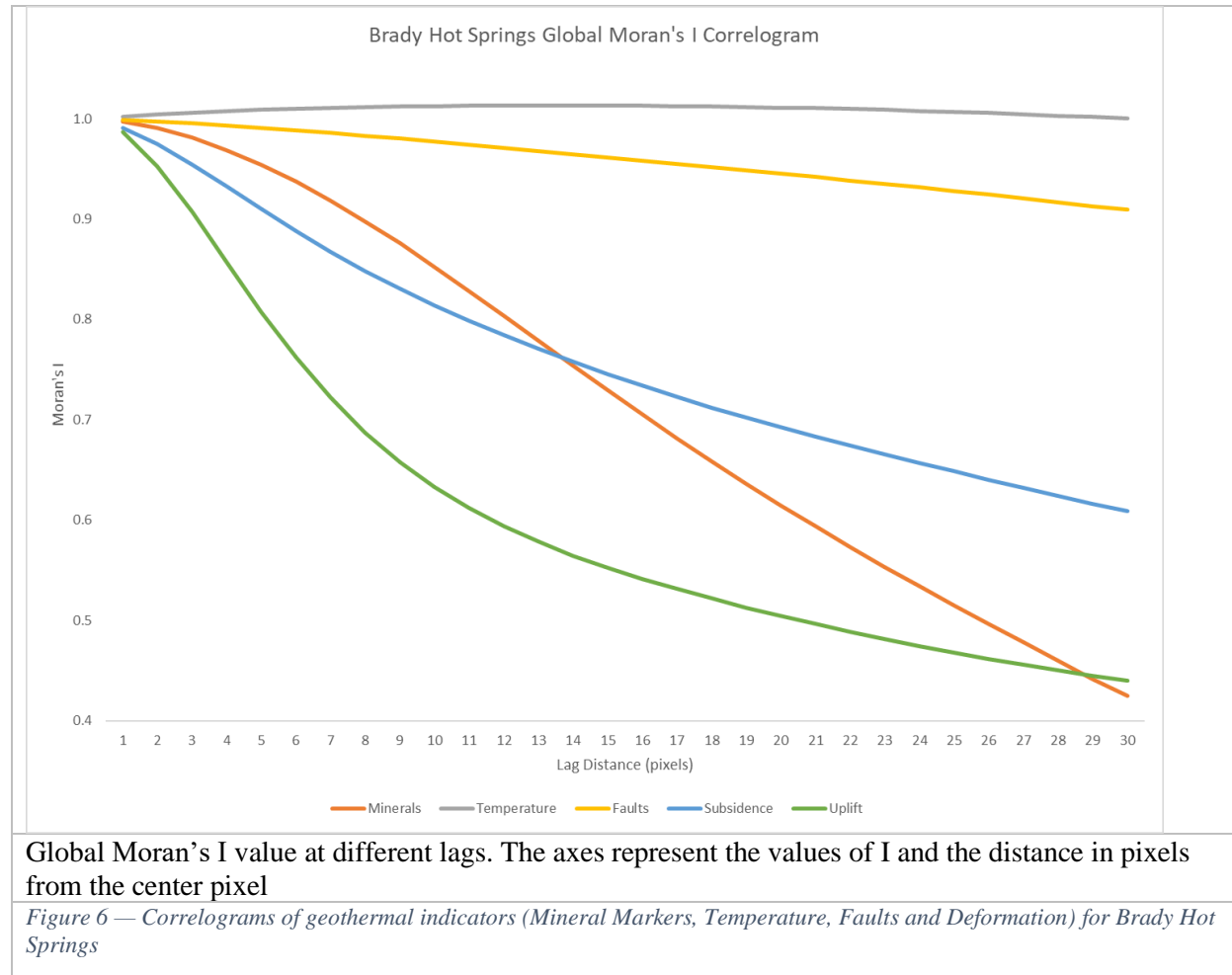


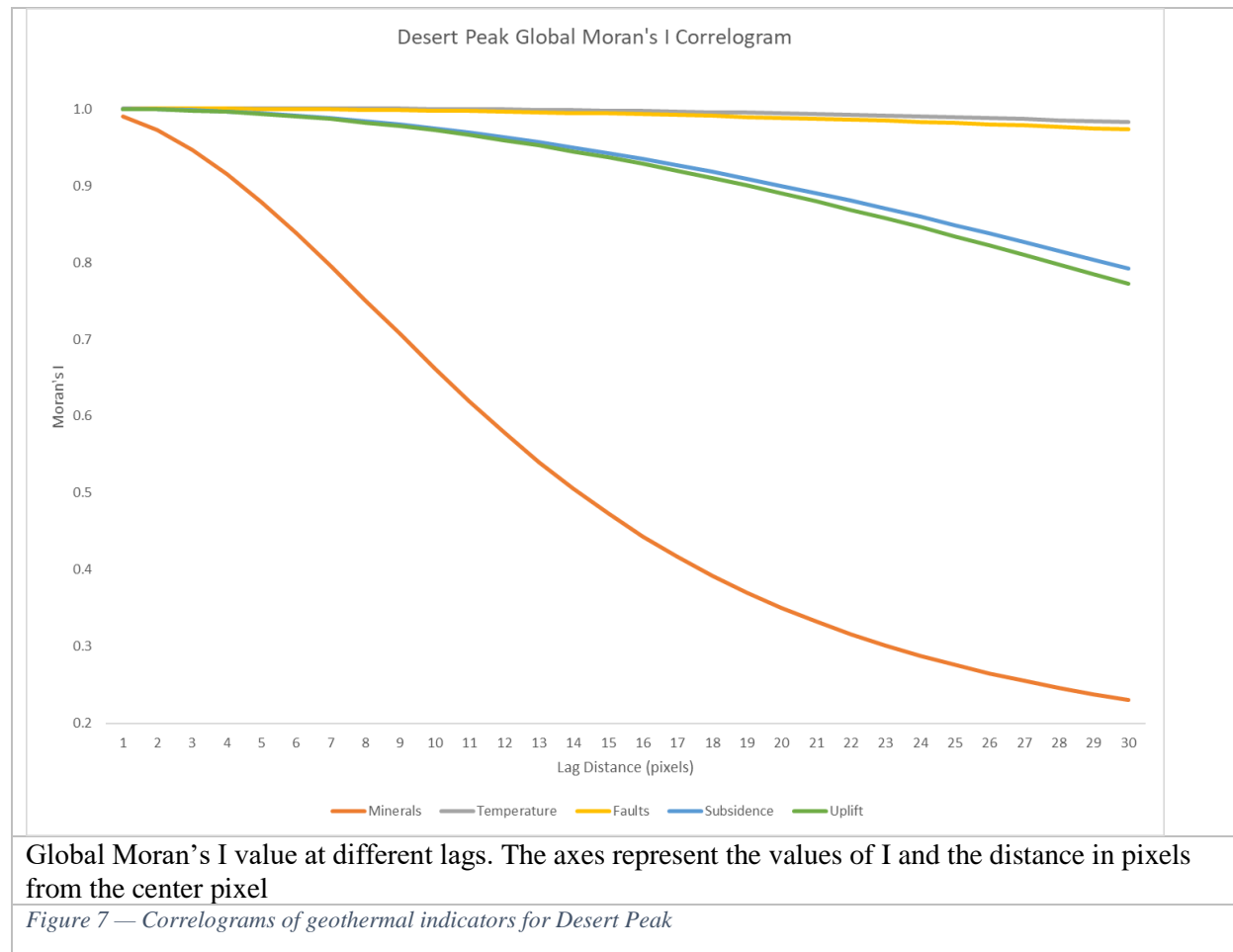
## 2.4. The Geothermal AI

Several studies used ML and heuristic methods to analyze geothermal potential for large regions. The decision trees and deep networks (15), Model Analysis and Decision Support (MADS) (30), Weight of Evidence (WoE), Bayesian inspired models (89), fuzzy logic and binary index overlay (19) are the ones used for regional scales. Bayesian networks are also used for exploration of other renewable energy sources (90) (60), and it has also been used extensively in geosciences in general (see Dramsch for a thorough review of the last 70 years (91)). However, these models lack in considering the spatial correlation structure of the data sets. To develop an accountable Geothermal AI to analyze resource potential in local scale, spatial correlation structure of the data sets is needed to be understood. This can be done through the use of exploratory spatial data analyses mainly conducting autocorrelation analyses. Coolbaugh et al. performed such analyses for geothermal studies in the Great Basin (92), which is also applied in mineral exploration (93). The deep learning models (DLM) require building its architecture relevant to the data characteristics and selecting appropriate spatial filtering (94). Incorporation of spatial autocorrelation structure in developing the architecture of the DLM, which are mainly based on convolutional neural networks (CNN), has potential to improve the prediction potential. The use of spatial correlation metrics, namely Moran's I, Geary's C (95), semivariograms or correlograms (96) provides insight into the identification of the kernel size for CNNs.

### Analysis of Autocorrelation

In order to investigate the autocorrelation for the geothermal indicator data sets we adopted Moran's I measure. This measure indicates the scale of autocorrelation for each indicator data set. We used this scale in developing Geothermal AI architecture by using a kernel that captures the autocorrelation structure of the data. Examples used of Moran's I can be found from (97) and (98). We computed Moran's I value for various scales (lag sizes) and plotted them as correlograms (Figure 10) considering Deformation, Temperature, Faults, and Mineral Marker layers. As it can be seen from Figure 10 each pixel has a positive correlation with a lag of up to 13 pixels around it.

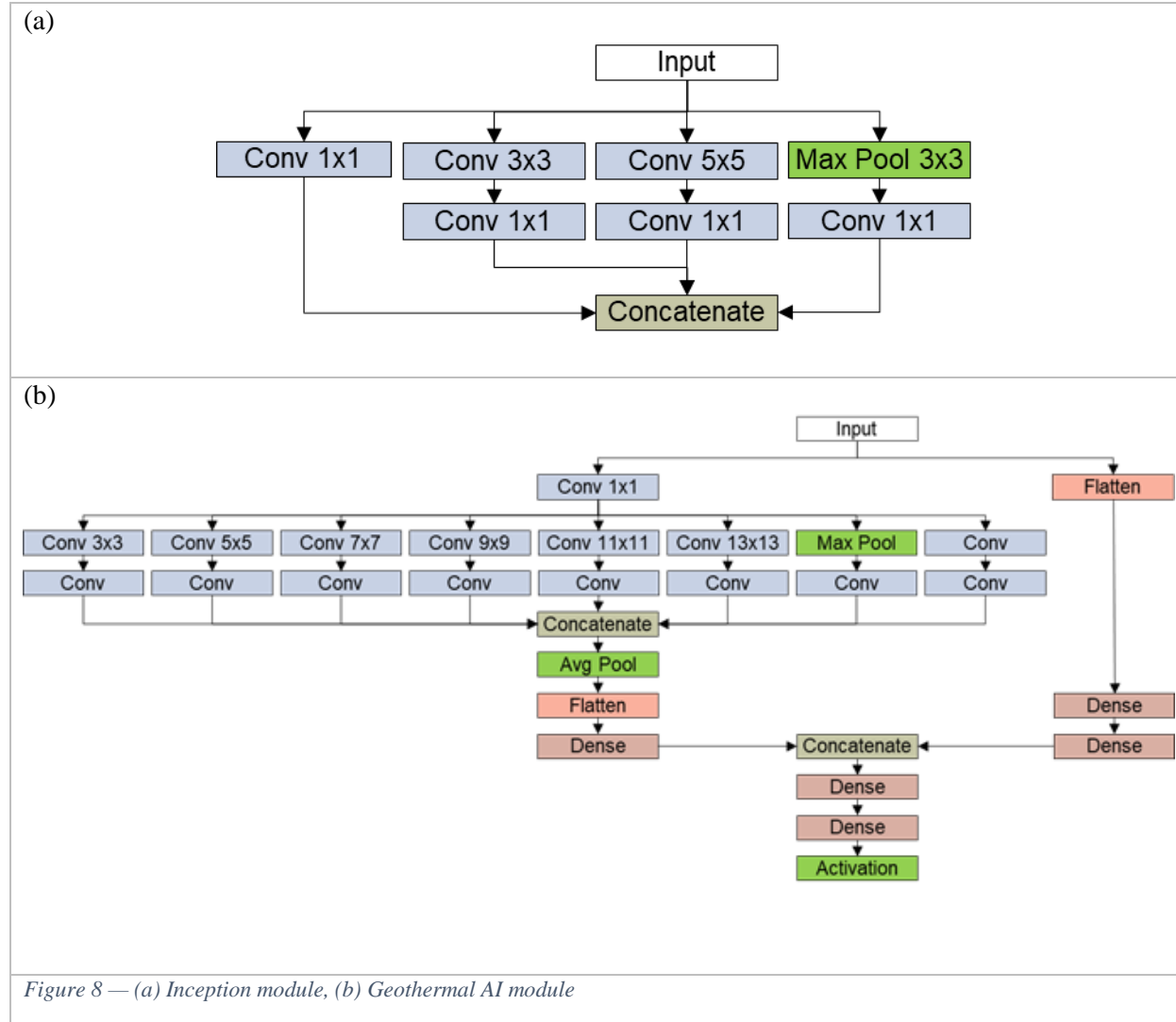




As it can be seen from Figure 6 and Figure 7, all indicators present positive autocorrelation, which becomes smaller based on distance. By pixel 9, the deformation indicators (Uplift and subsidence) show a steep drop, and in both sites the mineral markers indicator has an inflection point around pixel 13 or 14. Based on this analysis we can infer that the autocorrelation is stronger up to pixel 13, and this will be used as an input in the architecture design of the Geothermal AI.

#### Design of the Geothermal AI architecture

The Geothermal AI adopts the CNN algorithm and smaller kernels design of GoogleNet's Inception module (99) shown in Figure 8 (a). We modified original architecture of GoogleNet's Inception module (Figure 11a) by incorporating additional kernels based on the results of autocorrelation analyses. We implemented this new CNN architecture using Python 3.7, with the Tensorflow-GPU module.



The network of the Geothermal AI (Figure 8 (b)) uses two parallel blocks that are merged in the second concatenate layer. The first block (in the left side of the diagram, Figure 8 (b)) uses filters of different sizes to classify the inputs based on spatial information (e.g., patterns, textures). The second block (in the right side of the diagram, Figure 8 (b)) uses the whole image, but discards spatial information by flattening it. The objective of this approach is to ensure that not just the filters provide information, but also each pixel from each layer. This ensures that no detailed information is lost when doing the final classification using dense layers (bottom of Figure 8 b).

The network contains standard TensorFlow layers (100) that perform different functions, in Figure 8 each type of layer has a different color to make it easier to identify their type:

**Convolutional Layer (Conv):** It implements 2D convolutions using the kernel size defined in the layer description (e.g., Conv 13x13 would implement a convolution in the image using a kernel of 13 by 13 nodes). Convolutions perform the task of filters in an image, and the learning process changes the layer to obtain best fit filters that match the relevant image textures.

**Max Pooling (Max Pool):** The Max Pooling layer performs a voting mechanism based on the kernel size defined, where the output of the kernel corresponds to the maximum value of the input filtered by the kernel.

**Concatenate:** The concatenate layer merges the data into one single output, it is used to reduce dimensionality of the input.

**Average Pooling (Avg Pool):** The Average Pooling layers execute a kernel-based voting mechanism similar to Max Pool, except that the output corresponds to the average value of all the inputs.

**Flatten:** The Flatten layers reduce dimensionality of the inputs by turning any input matrix into a 1D vector of values. In this step, the multidimensional input (3D and 2D) loses its spatial components, but it can be rebuilt by resampling it into a matrix if required.

**Dense:** A Dense layer creates one-to-one connections between all its nodes and each one of the inputs, this ensures all inputs are used to calculate the output based on learned weights and bias.

**Activation Function:** In this last step, the inputs are turned into one or more outputs based on a selected activation function. In our case, we used SoftMax, which turns a continuous variable into a label (“Geothermal” or “Non-geothermal”).

### Training and testing

We first trained the developed architecture for Brady site. We partitioned the overall pixels in the AOI (592,898 pixels) into training (6.7 %), validation (6.7 %) and testing (20.2 %) pixels. The training data set is prepared using the tiles having 19 by 19 pixels. We used the first layers as input, and the label layer as the expected output.

Then we separately trained Desert Peak site by partitioning the overall pixels in the AOI (2,533,789 pixels) into training (1.6 %), validation (1.6 %) and testing (4.7 %) pixels.

We trained the Geothermal AI using High Performance Computing (HPC) resources of Colorado School of Mines, in a single Penguin Computing Relion XO1114GTS GPU Node, with 192 GB RAM and 4 NVIDIA Tesla V100-SXM2 (32GB HBM2, 5120 CUDA, 640 Tensor). The Operating System used was CentOS 7, and the 10.1 CUDA Library. We conducted the for 100 epochs using augmentation of the data by rotating and mirroring the tiles. The accuracy metrics of the Geothermal AI for each site is given in Table 2.

*Table 2 — Performance of the Geothermal AI for the selected sites*

<b>Model</b>	<b>Non-Geothermal</b>			<b>Geothermal</b>			<b>Training Time</b>
	Accuracy	Precision	Recall	Precision	Recall		
<b>Brady</b>	95.5%	95%	96%	96%	95%	52'17"	
<b>Desert P.</b>	92.3%	91%	94%	94%	91%	49'16"	

The prediction maps using the geothermal AI for Brady and Desert Peak are given in Figure 9 and Figure 10,

As it can be seen from Figure 9, the prediction map for Brady shows that the prediction (pink), fits very well the labeled data (green). The Geothermal AI tends to ignore the isolated points outside of the geothermal plant's operations grounds. This may indicate that, potentially, the salt and pepper error in labeling is being ignored (isolated green patches in Figure 9, and blue dots outside of the magenta region in Figure 10). For the prediction map of Desert Peak (Figure 10), the prediction in blue overlaps almost all of the regions labeled (magenta). Similar to the Brady case, the fact that the Geothermal AI ignores patches outside of the core of the operation indicates the robustness of the developed Geothermal AI.

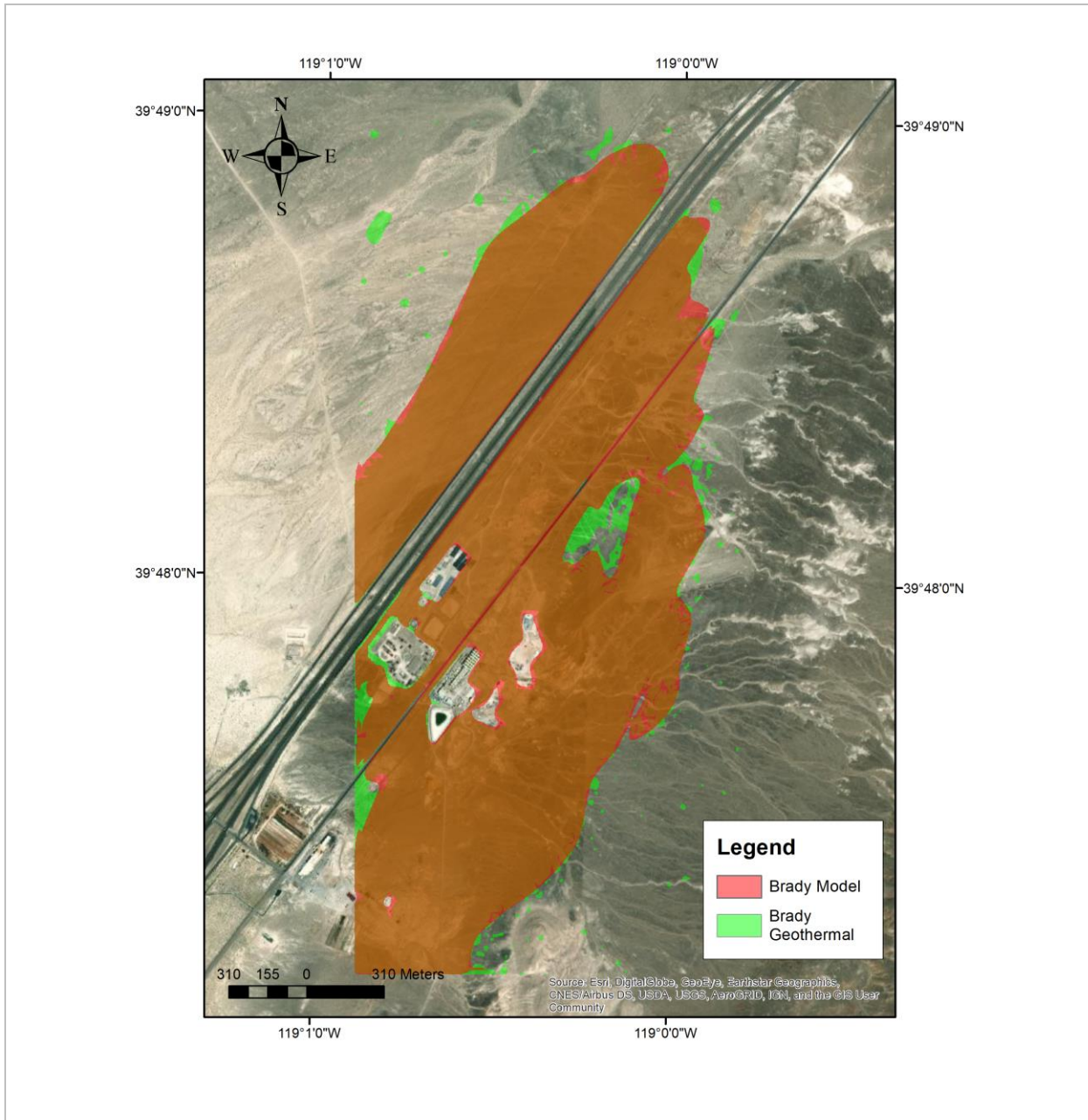


Figure 9 — Ground truth and prediction for Brady Hot Springs

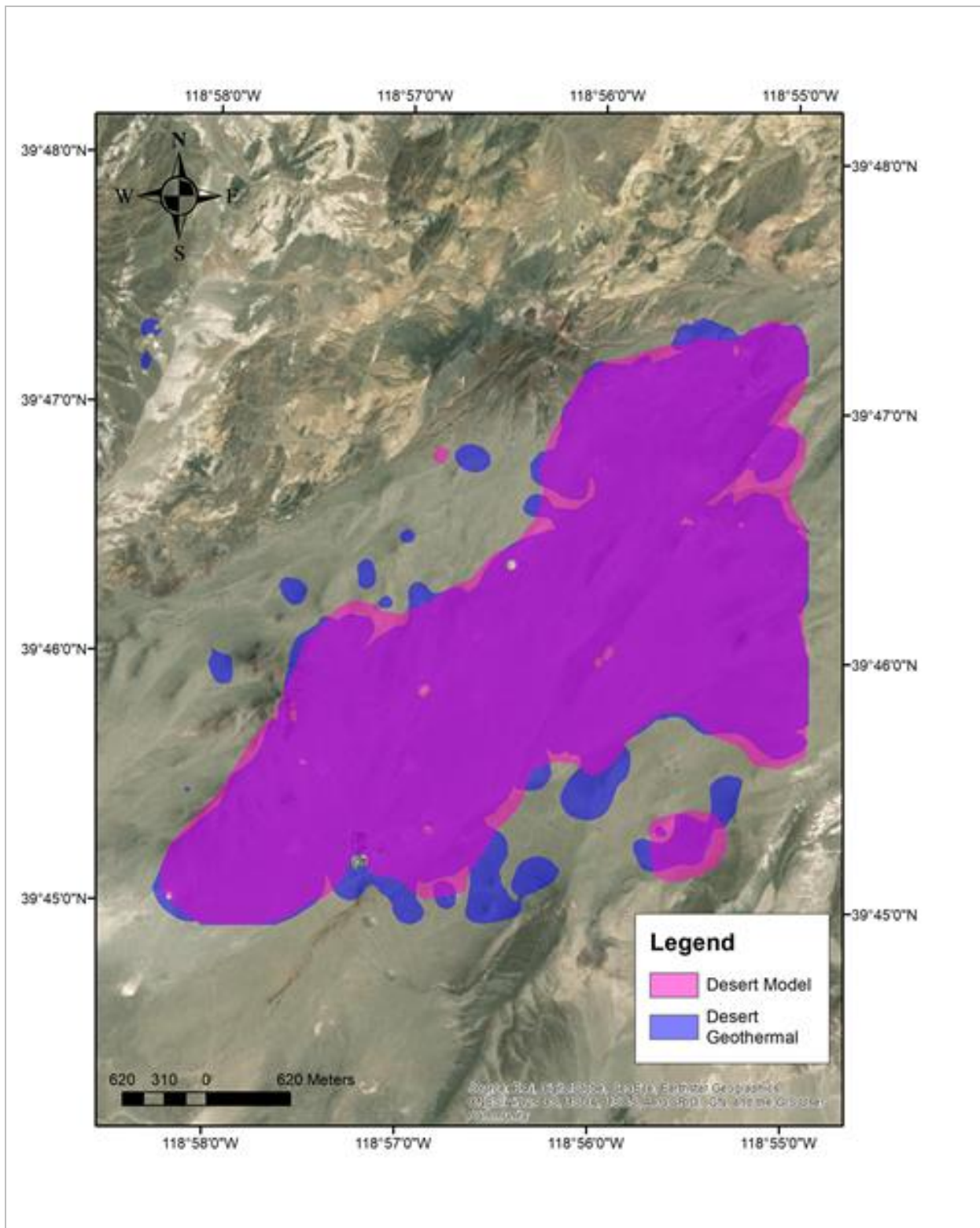


Figure 10 — Ground truth and prediction for Desert Peak

## 2.5. Accuracy Assessment

The results of the training and testing show that, for both models, the accuracy is over 90%. Moreover, even for the blind site (Desert Peak) the drop in accuracy is not large. In particular, the non-geothermal recall results show that the accuracy in properly classifying all non-geothermal points is 94%, but lower precision indicates a larger number of false negatives. To test the ability of each model to generalize, we applied the trained model of Brady to Desert Peak (test site) and the trained model of the Desert Peak to Brady (test site) without introducing and training data for the test sites. The performance metrics for this independent testing is given in Table 3.

Table 3 — Independent test performance of the Geothermal AI

Model	Applied to	Accuracy*	Non-Geothermal		Geothermal	
			Precision	Recall	Precision	Recall
<b>Brady</b>	Desert P.	72.4%	66%	97%	94%	46%
<b>Desert P.</b>	Brady	76.3%	72%	79%	81%	74%

(\*) When applying to a different site, all points in the tested site are used

Although there are significant differences in the geothermal characteristics of both sites, especially being Desert Peak a blind geothermal resource, the independent testing yields very good prediction maps (Figure 11 and Figure 12).

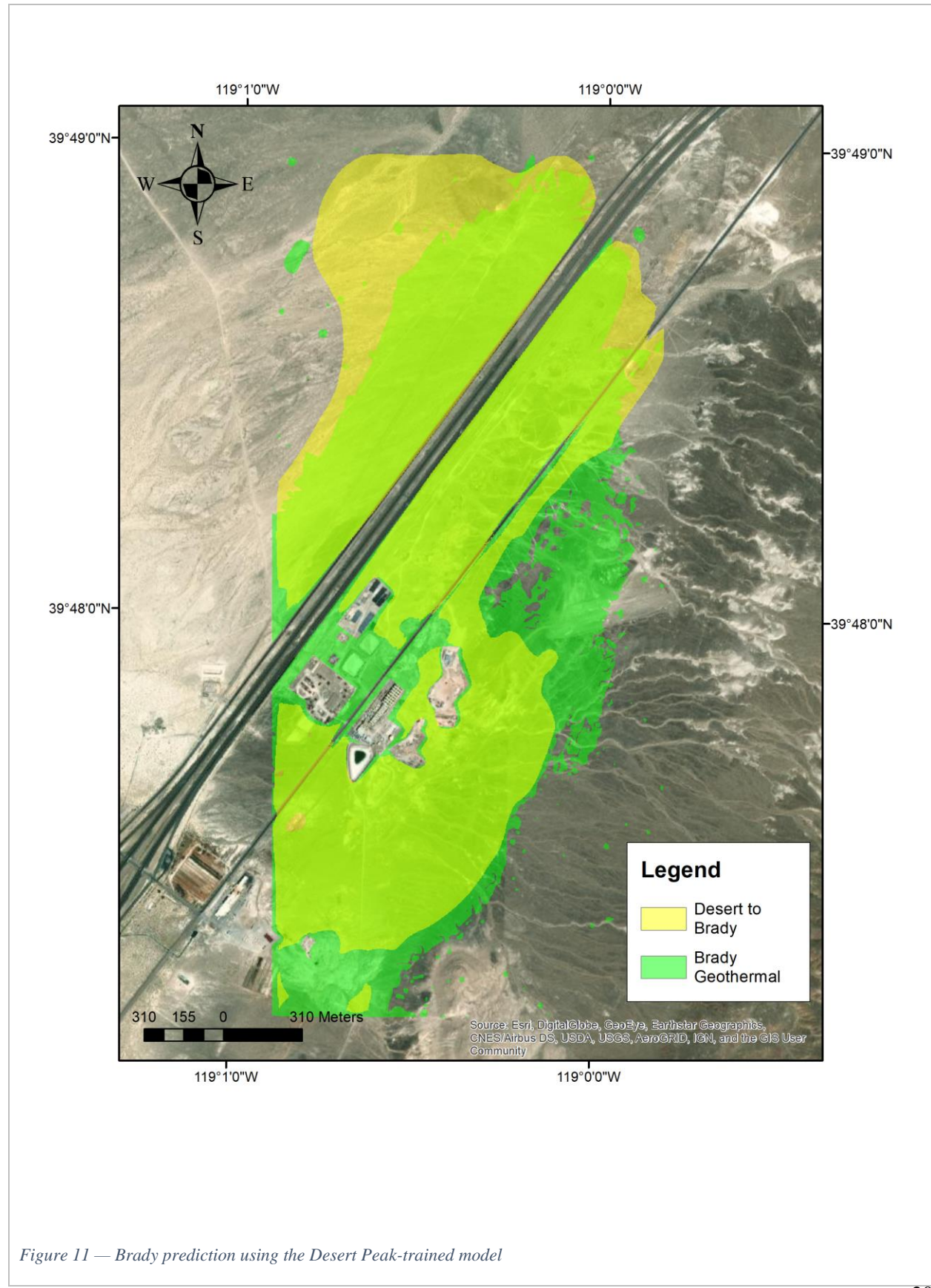


Figure 11 — Brady prediction using the Desert Peak-trained model

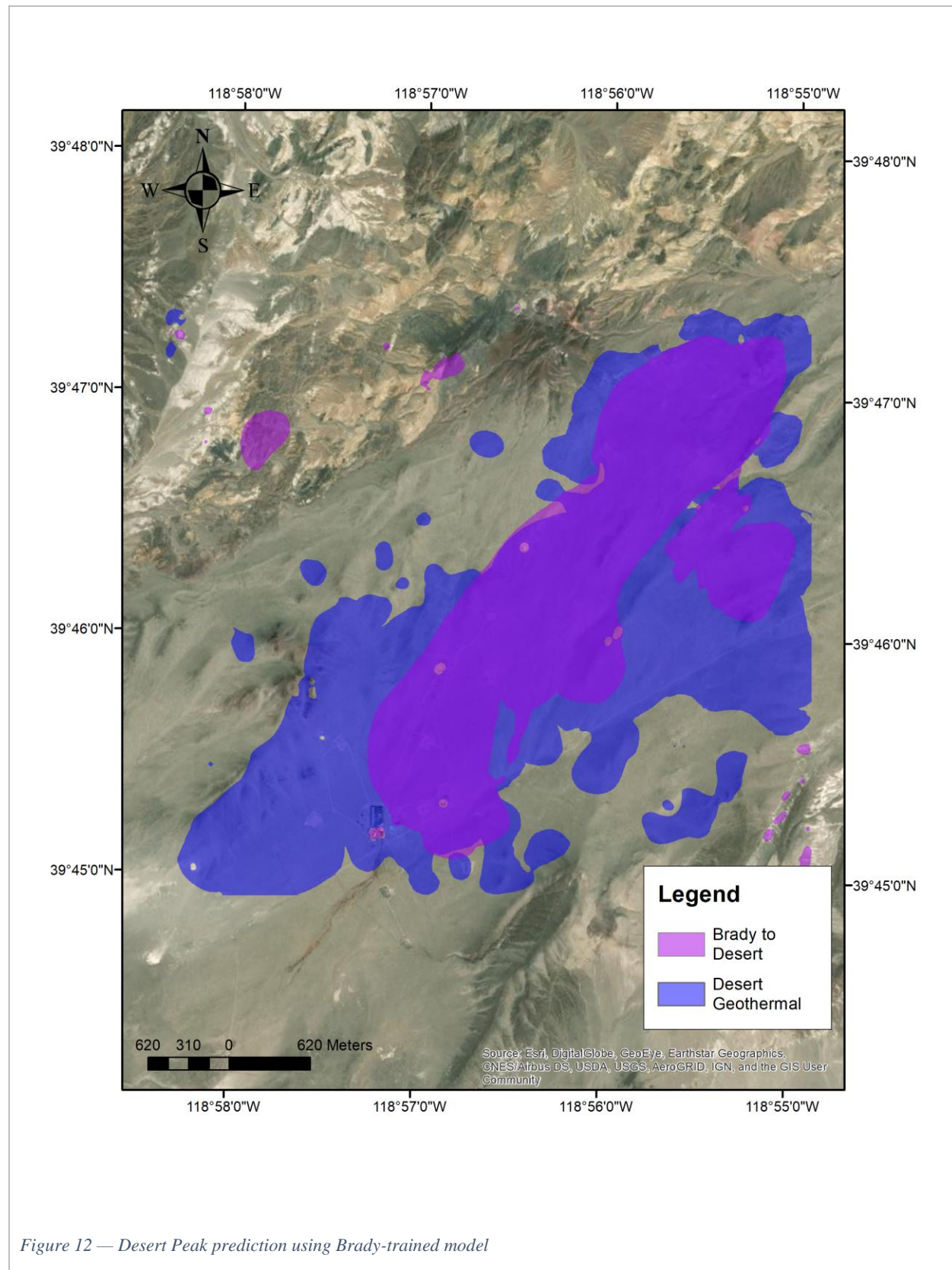


Figure 12 — Desert Peak prediction using Brady-trained model

### 3. Conclusions

Geothermal energy has not been adopted at the same pace of other renewable energy technologies, due to geological, economic and technological uncertainties that cause reduced investments. To decrease the cost and risk of projects, methods for reducing uncertainty in exploration of geothermal resources are needed. Recent developments in RS, ML and AI provide opportunities for leveraging the geothermal energy utilization. The existing research using these methods mainly consider large regions and also does not significantly exploit the integration of RS, ML and AI.

Our approach integrates RS, ML and AI for predicting the potential geothermal sites, that can be used not only for exploration of new sites but also expansion of existing sites. By partitioning and augmenting the data, we used less than 7% of the original data to train two models, namely Brady which has clear surface manifestations (fumaroles, hot springs, mud pools) and Desert Peak which is a blind site.

The Geothermal AI also makes use of analysis from spatial statistics to inform its architecture, which includes CNN kernels of dimensions 1x1, 3x3, 5x5, 7x7, 9x9, 11x11, and 13x13 for input images of 19x19x3 (3 channels of 19x19 pixels each). This architecture is based on the known image object recognition Inception module, which is suited for image pattern analysis (99) and has been used with modifications for hyperspectral analysis (101).

The results show that the Geothermal AI achieves an accuracy level between 92 and 95%, with the lower accuracy belonging to the blind site (Desert Peak). Moreover, when using the trained models on the opposite sites the accuracy varies between 72 and 76%. Furthermore, the Geothermal AI predicts a considerable area of footprint that matches the main regions of each considered geothermal site.

The Geothermal AI tends to cluster the data, and the prediction reduces some of the probable salt-and-pepper errors introduced by the automated labeling. This also shows the robustness of the proposed approach. The Geothermal AI produces conservative results, with precision of 94 and 96% for pixels labeled as geothermal for the same site, and a precision between 81 and 94% when it is used in a different site. These promising results demonstrate that even with a low number of input layers (temperature, fault density, and mineral markers), the Geothermal AI can be applicable to other sites.

The model is geared towards the early stages of exploration and it only finds the footprint of the geothermal resource and not its potential. To find the total capacity of the geothermal source, a subsurface model is needed and the authors are adapting the model for subsurface prediction to predict/assess total capacity.

Future research should include adding more available RS data, increasing the depth of the network, trying different or a refined version of the labeling algorithm that makes use of self-training data for brownfield sites, and incorporating subsurface data and models when available.

### Acknowledgements

This project has been funded by the US Department of Energy grant number DE- EE0008760, made use of the High-Performance Computing (HPC) and other facilities at the Colorado School of Mines, and benefitted from the availability of satellite data from ESA's Sentinel and NASA's LANDSAT projects, the geological information from the Nevada Bureau of Mines and Geology, and USGS. Additionally, we would like to thank professor Ge Jin, Assistant Professor of Geophysics at Colorado School of Mines, for his input in the selection of layers for the AI.

## List of References

1. Davenport C. Nations Approve Landmark Climate Accord in Paris. *The New York Times* [Internet]. 2015 Dec 12 [cited 2021 Feb 11]; Available from: <https://www.nytimes.com/2015/12/13/world/europe/climate-change-accord-paris.html>
2. Independent Group of Scientists appointed by the Secretary-General. *Global Sustainable Development Report 2019: The Future is Now – Science for Achieving Sustainable Development* [Internet]. New York: United Nations; 2019 [cited 2021 Feb 11]. Available from: [https://sustainabledevelopment.un.org/content/documents/24797GSDR\\_report\\_2019.pdf](https://sustainabledevelopment.un.org/content/documents/24797GSDR_report_2019.pdf)
3. Xia L, Zhang Y. An overview of world geothermal power generation and a case study on China—The resource and market perspective. *Renewable and Sustainable Energy Reviews*. 2019 Sep 1;112:411–23.
4. Sanchez-Alfaro P, Sielfeld G, Campen BV, Dobson P, Fuentes V, Reed A, et al. Geothermal barriers, policies and economics in Chile – Lessons for the Andes. *Renewable and Sustainable Energy Reviews*. 2015 Nov 1;51:1390–401.
5. Clauser C, Ewert M. The renewables cost challenge: Levelized cost of geothermal electric energy compared to other sources of primary energy – Review and case study. *Renewable and Sustainable Energy Reviews*. 2018 Feb 1;82:3683–93.
6. Ray D. Lazard's Levelized Cost of Energy Analysis—Version 14.0 [Internet]. 2020 [cited 2021 Feb 11] p. 21. Available from: <https://www.lazard.com/media/451419/lazards-levelized-cost-of-energy-version-140.pdf>
7. IRENA. Renewable Power Generation Costs in 2019 [Internet]. 2020 [cited 2021 Feb 10]. 144 p. Available from: [https://www.irena.org/-/media/Files/IRENA/Agency/Publication/2020/Jun/IRENA\\_Power\\_Generation\\_Costs\\_2019.pdf](https://www.irena.org/-/media/Files/IRENA/Agency/Publication/2020/Jun/IRENA_Power_Generation_Costs_2019.pdf)
8. Akar S, Young KR (ORCID:0000000290689731). Assessment of New Approaches in Geothermal Exploration Decision Making: Preprint [Internet]. National Renewable Energy Lab. (NREL), Golden, CO (United States); 2015 Feb [cited 2021 Feb 11]. Report No.: NREL/CP-6A20-63546. Available from: <https://www.osti.gov/biblio/1171791>
9. Hervey C, Beardsmore G, Moeck I, Ruter H, Bauer S. Best practices guide for geothermal exploration [Internet]. Washington, D.C.: The World Bank; 2014 Jun [cited 2021 Feb 11]. Report No.: 110532. Available from: <https://documents.worldbank.org/en/publication/documents-reports/documentdetail/190071480069890732/Best-practices-guide-for-geothermal-exploration>
10. van der Zwaan B, Dalla Longa F. Integrated assessment projections for global geothermal energy use. *Geothermics*. 2019 Nov 1;82:203–11.
11. Serdjuk M, Dumas L, Angelino L, Tryggvadóttir L. Geothermal investment guide. GEOELEC project report (European Union). 2013;40.
12. Witter JB, Trainor-Guitton WJ, Siler DL. Uncertainty and risk evaluation during the exploration stage of geothermal development: A review. *Geothermics*. 2019 Mar 1;78:233–42.

13. van der Meer F, Hecker C, van Ruitenbeek F, van der Werff H, de Wijkerslooth C, Wechsler C. Geologic remote sensing for geothermal exploration: A review. *International Journal of Applied Earth Observation and Geoinformation*. 2014 Dec 1;33:255–69.
14. Faulds JE, Hinz NH, Coolbaugh MF, Shevenell LA, Siler DL. The Nevada Play Fairway Project—Phase II: Initial Search for New Viable Geothermal Systems in the Great Basin Region, Western USA. *Geothermal Resources Council Transactions*. 2016;40:535–40.
15. Faulds JE, Brown S, Coolbaugh M, Deangelo J, Queen J, Treitel S, et al. Preliminary Report on Applications of Machine Learning Techniques to the Nevada Geothermal Play Fairway Analysis. 2020.
16. Hase H, Miyazaki Y. Geothermal resources map aided by remote sensing data. *Proceedings of international archives of photogrammetry and remote sensing*. 1988;27:212–21.
17. Littlefield EF, Calvin WM. Geothermal exploration using imaging spectrometer data over Fish Lake Valley, Nevada. *Remote Sensing of Environment*. 2014 Jan 1;140:509–18.
18. Calvin WM, Pace EL. Mapping alteration in geothermal drill core using a field portable spectroradiometer. *Geothermics*. 2016 May 1;61:12–23.
19. Sadeghi B, Khalajmasoumi M. A futuristic review for evaluation of geothermal potentials using fuzzy logic and binary index overlay in GIS environment. *Renewable and Sustainable Energy Reviews*. 2015 Mar 1;43:818–31.
20. Lösing M, Ebbing J. Predicting Geothermal Heat Flow in Antarctica With a Machine Learning Approach. *Journal of Geophysical Research: Solid Earth*. 2021;126(6):e2020JB021499.
21. Zheng Y, Li J, Lin R, Hu H, Gao K, Huang L. Physics-guided machine learning approach to characterizing small-scale fractures in geothermal fields. In: Proceedings, forty-sixth workshop on geothermal reservoir engineering, Stanford University. 2021. p. 9.
22. Shahdi A, Lee S, Karpatne A, Nojabaei B. Exploratory analysis of machine learning methods in predicting subsurface temperature and geothermal gradient of Northeastern United States. *Geothermal Energy*. 2021 Jul 2;9(1):18.
23. Tut Haklidir FS, Haklidir M. Prediction of geothermal originated boron contamination by deep learning approach: at Western Anatolia Geothermal Systems in Turkey. *Environ Earth Sci*. 2020 Apr 8;79(8):180.
24. Tut Haklidir F, Haklidir M. The Reservoir Temperature Prediction Using Hydrogeochemical Indicators By Machine Learning: Western Anatolia (Turkey) Case. In: Proceedings World Geothermal Congress. 2021. p. 1.
25. Duplyakin D, Beckers KF, Siler DL, Martin MJ, Johnston HE. Modeling Subsurface Performance of a Geothermal Reservoir Using Machine Learning. *Energies*. 2022 Jan;15(3):967.
26. Buster G, Siratovich P, Taverna N, Rossol M, Weers J, Blair A, et al. A New Modeling Framework for Geothermal Operational Optimization with Machine Learning (GOOML). *Energies*. 2021 Jan;14(20):6852.

27. Muther T, Syed FI, Lancaster AT, Salsabila FD, Dahaghi AK, Negahban S. Geothermal 4.0: AI-enabled geothermal reservoir development- current status, potentials, limitations, and ways forward. *Geothermics*. 2022 Mar 1;100:102348.
28. Liu R, Misra S. Machine Learning Assisted Exploration and Production of Subsurface Energy and Carbon Geo-Sequestration: A Review. *Earth and Space Science Open Archive*. 2020;56.
29. Vesselinov VV, O'Malley D, Frash LP, Ahmmed B, Rupe AT, Karra S, et al. Geo Thermal Cloud: Cloud Fusion of Big Data and Multi-Physics Models using Machine Learning for Discovery, Exploration, and Development of Hidden Geothermal Resources [Internet]. Los Alamos National Lab. (LANL), Los Alamos, NM (United States); 2021 May [cited 2022 Feb 16]. Report No.: LA-UR-21-24325. Available from: <https://www.osti.gov/biblio/1782607>
30. Vesselinov VV, Mudunuru MK, Ahmmed B, Karra S, Middleton RS. Discovering Signatures of Hidden Geothermal Resources Based on Unsupervised Learning. In: *PROCEEDINGS, 45th Workshop on Geothermal Reservoir Engineering* [Internet]. Stanford, California, United States; 2020. p. 9. Available from: <https://permalink.lanl.gov/object/tr?what=info:lanl-repo/lareport/LA-UR-20-21030>
31. Ahmmed B, Vesselinov VV, Mudunuru MK, Middleton R, Karra S. Machine Learning on the Geochemical Characteristics of Low-, Medium-, and Hot-temperature Geothermal Resources in the Great Basin, USA. Los Alamos National Lab.(LANL), Los Alamos, NM (United States); 2021.
32. Ahmmed B, Lautze N, Vesselinov VV, Dores D, Mudunuru MK. Unsupervised machine learning to extract dominant geothermal attributes in Hawaii Island Play Fairway data. Los Alamos National Lab.(LANL), Los Alamos, NM (United States); 2021.
33. Ahmmed B, Vesselinov V. Prospectivity Analyses of the Utah FORGE Site using Unsupervised Machine Learning. 2021.
34. Smith CM, Faulds JE, Brown S, Coolbaugh M, Lindsey CR, Treitel S, et al. Characterizing Signatures of Geothermal Exploration Data with Machine Learning Techniques: An Application to the Nevada Play Fairway Analysis. *46th Workshop on Geothermal Reservoir Engineering*, Stanford University, California, SGP-TR-218. 2021;
35. Brady Hot Springs Geothermal Area [Internet]. Open Energy Information. [cited 2021 Feb 17]. Available from: [https://openei.org/wiki/Brady\\_Hot\\_Springs\\_Geothermal\\_Area](https://openei.org/wiki/Brady_Hot_Springs_Geothermal_Area)
36. Desert Peak Geothermal Area [Internet]. Open Energy Information. [cited 2021 Feb 17]. Available from: [https://openei.org/wiki/Desert\\_Peak\\_Geothermal\\_Area](https://openei.org/wiki/Desert_Peak_Geothermal_Area)
37. Ciriaco AE, Zarrouk SJ, Zakeri G. Geothermal resource and reserve assessment methodology: Overview, analysis and future directions. *Renewable and Sustainable Energy Reviews*. 2020 Mar 1;119:109515.
38. Faulds JE, Craig JW, Coolbaugh M, Hinz N, Glen JM, Deoreo S. Searching for Blind Geothermal Systems Utilizing Play Fairway Analysis, Western Nevada [Internet]. 2018 [cited 2020 Dec 5]. Available from: [/paper/Searching-for-Blind-Geothermal-Systems-Utilizing-%2C-James-Craig/d3a97875412d704befcacc2c3614c15726fdcadd](https://paper/Searching-for-Blind-Geothermal-Systems-Utilizing-%2C-James-Craig/d3a97875412d704befcacc2c3614c15726fdcadd)

39. Jennejohn D. Research and Development in Geothermal Exploration and Drilling [Internet]. Geothermal Energy Association; 2009 Dec p. 1–25. Available from: [https://www.mtprincetongeothermal.com/wp-content/uploads/2011/03/Res-Develop-Geothermal-Exploration-Drilling\\_2009.pdf](https://www.mtprincetongeothermal.com/wp-content/uploads/2011/03/Res-Develop-Geothermal-Exploration-Drilling_2009.pdf)
40. Henley RW, Ellis AJ. Geothermal systems ancient and modern: a geochemical review. *Earth-Science Reviews*. 1983 Jan 1;19(1):1–50.
41. Mokhtari Z, Boomeri M, Bagheri S. Digital Image Processing and Analysis Techniques for Detection of Hydrothermal Alteration Zones: A Case Study in Siah-Jangal Area, North of Taftan Volcano, Southeastern Iran. *Journal of the Indian Society of Remote Sensing*. 2015 Jun 1;43.
42. Huntington JF. The Role of Remote Sensing in Finding Hydrothermal Mineral Deposits on Earth. *Ciba Foundation symposium*. 1996 Feb 1;202:214–31; discussion 231.
43. Lynne BY, Campbell KA. Diagenetic transformations (opal-A to quartz) of low- and mid-temperature microbial textures in siliceous hot-spring deposits, Taupo Volcanic Zone, New Zealand. *Canadian Journal of Earth Sciences*. 2003 Nov 1;40(11):1679–96.
44. Livo K, Kruse F, Clark R, Kokaly R, Shanks W. Hydrothermally Altered Rock and Hot-Spring Deposits at Yellowstone National Park—Characterized Using Airborne Visible- and Infrared-Spectroscopy Data. *Publications of the US Geological Survey* [Internet]. 2007 Jan 1; Available from: <https://digitalcommons.unl.edu/usgspubs/74>
45. Inostroza M, Tassi F, Sepúlveda J, Capecchiacci F, Rizzo AF, Aguilera F. Geochemical survey of the Colpitas-Taapaca volcanic-hydrothermal system, northern Chile. *Italian Journal of Geosciences*. 2020 Oct 1;139(3):359–73.
46. Barbour AJ, Evans EL, Hickman SH, Eneva M. Subsidence rates at the southern Salton Sea consistent with reservoir depletion. *Journal of Geophysical Research: Solid Earth*. 2016;121(7):5308–27.
47. Gaucher E, Schoenball M, Heidbach O, Zang A, Fokker PA, van Wees J-D, et al. Induced seismicity in geothermal reservoirs: A review of forecasting approaches. *Renewable and Sustainable Energy Reviews*. 2015 Dec 1;52:1473–90.
48. Abdel Zaher M, Saibi H, Mansour K, Khalil A, Soliman M. Geothermal exploration using airborne gravity and magnetic data at Siwa Oasis, Western Desert, Egypt. *Renewable and Sustainable Energy Reviews*. 2018 Feb 1;82:3824–32.
49. Aretouyap Z, Nouck PN, Nouayou R. A discussion of major geophysical methods used for geothermal exploration in Africa. *Renewable and Sustainable Energy Reviews*. 2016 May 1;58:775–81.
50. Domra Kana J, Djongyang N, Danwe Raïdandi, Njandjock Nouck P, Abdouramani Dadjé. A review of geophysical methods for geothermal exploration. *Renewable and Sustainable Energy Reviews*. 2015 Apr 1;44:87–95.
51. Wang W, Diessl J, Bruno MS. Surface deformation study for a geothermal operation field. *Adv Geosci*. 2018 Sep 4;45:243–9.

52. Reath KA, Ramsey MS. Exploration of geothermal systems using hyperspectral thermal infrared remote sensing. *Journal of Volcanology and Geothermal Research*. 2013 Sep;265:27–38.
53. Pirajno F. Subaerial hot springs and near-surface hydrothermal mineral systems past and present, and possible extraterrestrial analogues. *Geoscience Frontiers*. 2020 Sep 1;11(5):1549–69.
54. Kratt C, Calvin W, Coolbaugh M. Geothermal exploration with Hymap hyperspectral data at Brady–Desert Peak, Nevada. *Remote Sensing of Environment*. 2006 Oct 15;104(3):313–24.
55. Kratt C, Calvin WM, Coolbaugh MF. Mineral mapping in the Pyramid Lake basin: Hydrothermal alteration, chemical precipitates and geothermal energy potential. *Remote Sensing of Environment*. 2010 Oct 15;114(10):2297–304.
56. Faulds JE, Ramelli AR, Garside LJ, Coolbaugh MF, Green HL. Preliminary geologic map of the Desert Peak quadrangle, Churchill County, Nevada [Internet]. 2012 [cited 2021 Feb 17]. (Open-File Report 2012-05). Available from: [https://data.nbmng.unr.edu/public/freedownloads/geospatial-pdf/OF2012-05\\_plate.pdf](https://data.nbmng.unr.edu/public/freedownloads/geospatial-pdf/OF2012-05_plate.pdf)
57. Faulds JE, Ramelli AR, Coolbaugh MF, Hinz NH, Garside LJ, Queen JH. Preliminary geologic map of the Bradys geothermal area, Churchill County, Nevada [Internet]. 2017 [cited 2021 Feb 17]. (Open-File Report 2017-04). Available from: [https://data.nbmng.unr.edu/public/freedownloads/geospatial-pdf/OF2012-05\\_plate.pdf](https://data.nbmng.unr.edu/public/freedownloads/geospatial-pdf/OF2012-05_plate.pdf)
58. Cardiff M, Feigl K, Zeng X, Lord N, Lancelle C, Parker LM, et al. Overview and Preliminary Results from the PoroTomo project at Brady Hot Springs, Nevada: Poroelastic Tomography by Adjoint Inverse Modeling of Data from Seismology, Geodesy, and Hydrology. In 2016.
59. Çavur M, Moraga J, Duzgun HS, Soydan H, Jin G. Displacement Analysis of Geothermal Field Based on PSInSAR And SOM Clustering Algorithms A Case Study of Brady Field, Nevada—USA. *Remote Sensing*. 2021 Jan 20;13(3):349.
60. Jha SKr, Bilalovic J, Jha A, Patel N, Zhang H. Renewable energy: Present research and future scope of Artificial Intelligence. *Renewable and Sustainable Energy Reviews*. 2017 Sep 1;77:297–317.
61. Alova G, Trotter PA, Money A. A machine-learning approach to predicting Africa’s electricity mix based on planned power plants and their chances of success. *Nat Energy*. 2021 Jan 11;1–9.
62. Paoletti M, Haut J, Plaza J, Plaza A. Deep learning classifiers for hyperspectral imaging: A review. *ISPRS Journal of Photogrammetry and Remote Sensing*. 2019 Dec 1;158:279–317.
63. Ganesan, B. S. Sathish, K. B. Shaik, V. Kalist. Neural network based SOM for multispectral image segmentation in RGB and HSV color space. In: 2015 International Conference on Circuits, Power and Computing Technologies [ICCPCT-2015]. 2015. p. 1–6.
64. Awad M. Segmentation of Satellite Images Using Self-Organizing Maps. In: Self-Organizing Maps [Internet]. INTECH Open Access Publisher; 2010. p. 430. Available from: <https://www.intechopen.com/books/self-organizing-maps/segmentation-of-satellite-images-using-self-organizing-maps>
65. Fu T. A review on time series data mining. *Engineering Applications of Artificial Intelligence*. 2011 Feb 1;24(1):164–81.

66. Hulle M. Chapter 1 Self-Organizing Maps [Internet]. 2009 [cited 2020 Dec 28]. Available from: [/paper/Chapter-1-Self-Organizing-Maps-Hulle/54d5ce0faf274b7bbdfa48a98493bd3c7f3fdc21](https://paper/Chapter-1-Self-Organizing-Maps-Hulle/54d5ce0faf274b7bbdfa48a98493bd3c7f3fdc21)
67. Liu H, Zhan Q, Yang C, Wang J. Characterizing the Spatio-Temporal Pattern of Land Surface Temperature through Time Series Clustering: Based on the Latent Pattern and Morphology. *Remote Sensing*. 2018 Apr;10(4):654.
68. Huang X, Ye Y, Xiong L, Lau RYK, Jiang N, Wang S. Time series k-means: A new k-means type smooth subspace clustering for time series data. *Information Sciences*. 2016 Nov 1;367–368:1–13.
69. Vaughan RG, Lowenstern JB, Keszthelyi LP, Jaworowski C, Heasler H. Mapping Temperature and Radiant Geothermal Heat Flux Anomalies in the Yellowstone Geothermal System Using ASTER Thermal Infrared Data. *GRC Transactions*. 2012;36:1403–10.
70. Howari F. Prospecting for geothermal energy through satellite based thermal data: Review and the way forward. *Global Journal of Environmental Science and Management*. 2015 Oct 1;1(4):265–74.
71. Kesler SE. Ore-Forming Fluids. *Elements*. 2005 Jan 1;1(1):13–8.
72. Helvacı C. Geological features of Neogene basins hosting borate deposits: an overview of deposits and future forecast, Turkey. *Bull Min Res Exp*. 2015;151(151):169–215.
73. Kokaly RF, Clark RN, Swayze GA, Livo KE, Hoefen TM, Pearson NC, et al. USGS spectral library version 7. US Geological Survey; 2017.
74. L3Harris Geospatial Solutions. ENVI - Environment for Visualizing Images [Internet]. L3Harris Geospatial Solutions. [cited 2020 Oct 27]. Available from: [https://www.l3harrisgeospatial.com/docs/using\\_envi\\_Home.html](https://www.l3harrisgeospatial.com/docs/using_envi_Home.html)
75. L3Harris Geospatial Solutions. Target Detection Wizard [Internet]. L3Harris Geospatial Solutions. 2020 [cited 2020 Oct 27]. Available from: <https://www.harrisgeospatial.com/docs/targetdetectionwizard.html>
76. Kraut S, Scharf LL, Butler RW. The Adaptive Coherence Estimator: A Uniformly Most-Powerful-Invariant Adaptive Detection Statistic. *IEEE Transactions on Signal Processing*. 2005 Feb;53(2):427–38.
77. Kelly EJ. An Adaptive Detection Algorithm. *IEEE Transactions on Aerospace and Electronic Systems*. 1986 Mar;AES-22(2):115–27.
78. Chang C-I, Liu J, Chieu B, Ren H, Wang C, Lo C, et al. Generalized constrained energy minimization approach to subpixel target detection for multispectral imagery. *Optical Engineering* [Internet]. 2000 May 1 [cited 2020 Oct 29];39. Available from: <http://adsabs.harvard.edu/abs/2000OptEn..39.1275C>
79. Turin G. An introduction to matched filters. *IRE Transactions on Information Theory*. 1960 Jun;6(3):311–29.
80. Chang C-I. Hyperspectral imaging: techniques for spectral detection and classification. Vol. 1. Springer Science & Business Media; 2003.

81. Kruse FA, Boardman JW. Fifteen Years of Hyperspectral Data: Northern Grapevine Mountains, Nevada. 1999 Feb;12.
82. Boardman J. Leveraging the High Dimensionality of AVIRIS Data for Improved Sub - Pixel Target Unmixing and Rejection of False Positives: Mixture Tuned Matched Filtering. Proceedings of the Seventh JPL Airborne Earth Science Workshop, JPL Publication. 1998;97–21.
83. Johnson SE. Constrained energy minimization and the target-constrained interference-minimized filter. *OE*. 2003 Jun;42(6):1850–4.
84. Ren H, Chang C-I. Target-constrained interference-minimized approach to subpixel target detection for hyperspectral images. *Optical Engineering - OPT ENG*. 2000 Dec 1;39(12):3138–45.
85. Parhami B. A taxonomy of voting schemes for data fusion and dependable computation. *Reliability Engineering & System Safety*. 1996 May 1;52(2):139–51.
86. Ferretti A, Prati C, Rocca F. Permanent scatterers in SAR interferometry. *IEEE Transactions on Geoscience and Remote Sensing*. 2001;39(1):8–20.
87. Ouali Y, Hudelot C, Tami M. An Overview of Deep Semi-Supervised Learning. *arXiv:200605278 [cs, stat] [Internet]*. 2020 Jul 6 [cited 2021 Feb 17]; Available from: <http://arxiv.org/abs/2006.05278>
88. Kohonen T. Self-organized formation of topologically correct feature maps. *Biological Cybernetics*. 1982;43(1):59–69.
89. Abuzied SM, Kaiser MF, Shendi E-AH, Abdel-Fattah MI. Multi-criteria decision support for geothermal resources exploration based on remote sensing, GIS and geophysical techniques along the Gulf of Suez coastal area, Egypt. *Geothermics*. 2020 Nov 1;88:101893.
90. Borunda M, Jaramillo OA, Reyes A, Ibargüengoytia PH. Bayesian networks in renewable energy systems: A bibliographical survey. *Renewable and Sustainable Energy Reviews*. 2016 Sep 1;62:32–45.
91. Dramsch JS. 70 years of machine learning in geoscience in review. In: *Advances in Geophysics*. 2020. p. 1–55.
92. Coolbaugh M, Zehner RE, Raines GL, Oppliger GL, Kreemer C. Regional prediction of geothermal systems in the Great Basin, USA using weights of evidence and logistic regression in a geographic information system (GIS). 2005 Jan 1;505–10.
93. Porwal A, Carranza EJM, Hale M. A Hybrid Fuzzy Weights-of-Evidence Model for Mineral Potential Mapping. *Nat Resour Res*. 2006 Mar 1;15(1):1–14.
94. Griffith D, Chun Y. Spatial autocorrelation and eigenvector spatial filtering. *Handbook of Regional Science*. 2014 Jan 1;1477–507.
95. Griffith DA. Spatial autocorrelation. Washington, DC: Association of American Geographers; 1987. (A Primer).
96. Curran PJ. The semivariogram in remote sensing: An introduction. *Remote Sensing of Environment*. 1988 Apr 1;24(3):493–507.

97. Espindola GM, Camara G, Reis IA, Bins LS, Monteiro AM. Parameter selection for region-growing image segmentation algorithms using spatial autocorrelation. *International Journal of Remote Sensing*. 2006 Jul 20;27(14):3035–40.
98. Boots B, Tiefelsdorf M. Global and local spatial autocorrelation in bounded regular tessellations. *J Geograph Syst*. 2000 Dec 1;2(4):319–48.
99. Szegedy C, Ioffe S, Vanhoucke V, Alemi A. Inception-v4, Inception-ResNet and the Impact of Residual Connections on Learning. *AAAI* [Internet]. 2017 Feb 12 [cited 2021 Feb 17];31(1). Available from: <https://ojs.aaai.org/index.php/AAAI/article/view/11231>
100. Module: tf.keras.layers | TensorFlow Core v2.4.1 [Internet]. TensorFlow. [cited 2021 Mar 9]. Available from: [https://www.tensorflow.org/api\\_docs/python/tf/keras/layers](https://www.tensorflow.org/api_docs/python/tf/keras/layers)
101. Kamat J, Gupta R. Inception SN: An Inception based Convolutional Neural Network for Hyperspectral Image Classification. 2020 Sep.